ISSN 1063-7834, Physics of the Solid State, 2006, Vol. 48, No. 6, pp. 1210–1213. © Pleiades Publishing, Inc., 2006.
Original Russian Text © E.D. Mishina, N.É. Sherstyuk, V.O. Val'dner, A.V. Mishina, K.A. Vorotilov, V.A. Vasil'ev, A.S. Sigov, M.P. De Santo, E. Cazzanelli, R. Barberi, Th. Rasing, 2006, published in Fizika Tverdogo Tela, 2006, Vol. 48, No. 6, pp. 1140–1142.

FILMS
AND NANOSTRUCTURES

Nonlinear-Optical and Micro-Raman Diagnostics of Thin Films and Nanostructures of ABO_3 Ferroelectrics

E. D. Mishina[a], N. É. Sherstyuk[a], V. O. Val'dner[a], A. V. Mishina[a], K. A. Vorotilov[a], V. A. Vasil'ev[a], A. S. Sigov[a], M. P. De Santo[b], E. Cazzanelli[b], R. Barberi[b], and Th. Rasing[c]

[a] *Moscow State Institute of Radio Engineering, Electronics, and Automation (Technical University), pr. Vernadskogo 78, Moscow, 119454 Russia*
e-mail: mishina_elena57@mail.ru
[b] *Università della Calabria, Arcavacata di Rende, Cosenza, 87036 Italy*
[c] *IMM, Radboud University Nijmegen, Toernooiveld 1, ED Nijmegen, 6525 Netherlands*

Abstract—Ferroelectric composite two-dimensional ferroelectric/aluminum oxide nanostructures were studied. A porous aluminum oxide matrix was used as a template into which a ferroelectric precursor was introduced, followed by annealing. The prepared nanostructures were studied using optical second harmonic generation and micro-Raman scattering.

PACS numbers: 77.84.Dy, 78.20.–e

DOI: 10.1134/S1063783406060618

1. INTRODUCTION

The matrix technique of nanostructure fabrication is based on the introduction of a ferroelectric material into a porous membrane. This technique allows fabrication of ferroelectric nanostructures with preset sizes, shape, and arrangement of individual nanoparticles. For example, ordered structures consisting of nanorods and nanotubes smaller than 1 μm in diameter have been obtained using the matrix technique [1].

In this paper, we describe the fabrication technique and present the results of studying nanostructures with significantly smaller sizes of nanoparticles fabricated from (Ba, Sr)TiO_3 (BST) and (Pb, Zr)TiO_3 (PZT) precursors introduced into pores of aluminum oxide membranes by the sol-gel method. It is shown that after annealing nanostructures exhibit ferroelectric properties, which manifest themselves in the optical properties of the nanostructures (second harmonic (SH) generation and Raman scattering (RS) spectra).

2. SAMPLE PREPARATION AND STRUCTURE

Composite nanostructures were fabricated using the conventional sol-gel technique applied to grow thin films [2]. Precursors BST (50/50) and PZT (53/47) were introduced into an Al_2O_3 porous membrane by immersing the membrane into a precursor followed by centrifugation. Two membrane types were used: membranes with pores 20–50 nm in size ordered into a hexagonal structure (M_1) and disordered membranes with pore sizes of 100–200 nm (M_2). The procedure was repeated three to five times and was followed by high-temperature annealing, under which a crystalline ferroelectric phase forms in films. The morphology of porous substrates and of nanostructures was studied by atomic-force microscopy (AFM). Figure 1 shows the AFM images of aluminum oxide membranes with various pore sizes (Figs. 1a, 1b) and nanostructures based on them (Figs. 1c, 1d). In membranes with small pores (50 nm in size), the fraction of filled pores is 50–60% (Fig. 1c). In membranes with large pores (100–200 nm, Fig. 1d), the fraction of filled pores is 100%; however, some nanoparticles are shaped like nanotubes rather than nanorods.

3. OPTICAL PROPERTIES

3.1. Nonlinear Optical Properties

The presence of the ferroelectric phase was checked using SH generation. Nanostructures with pore sizes of ~50 nm are transparent, and linear scattering in them is insignificant. For this reason, we studied the dependence of the SH intensity $I^{2\omega}(\alpha)$ on the angle of incidence in transmission (Fig. 2). Measurements were carried out using a femtosecond optical parametric amplifier (the wavelength range is 600–800 nm, the pulse duration is 200 fs, and the repetition rate is 1 kHz) and a photon counting system. The $I^{2\omega}(\alpha)$ dependences in annealed and unannealed samples were compared. In the former case, the $I^{2\omega}(\alpha)$ dependence exhibits two peaks: a peak I_1 at 40°–50° and a peak I_2 at 70°–80°. Peak I_2 increases in height with the wavelength of light. The unannealed structures exhibit only peak I_1, with its intensity being ten times lower than that for the

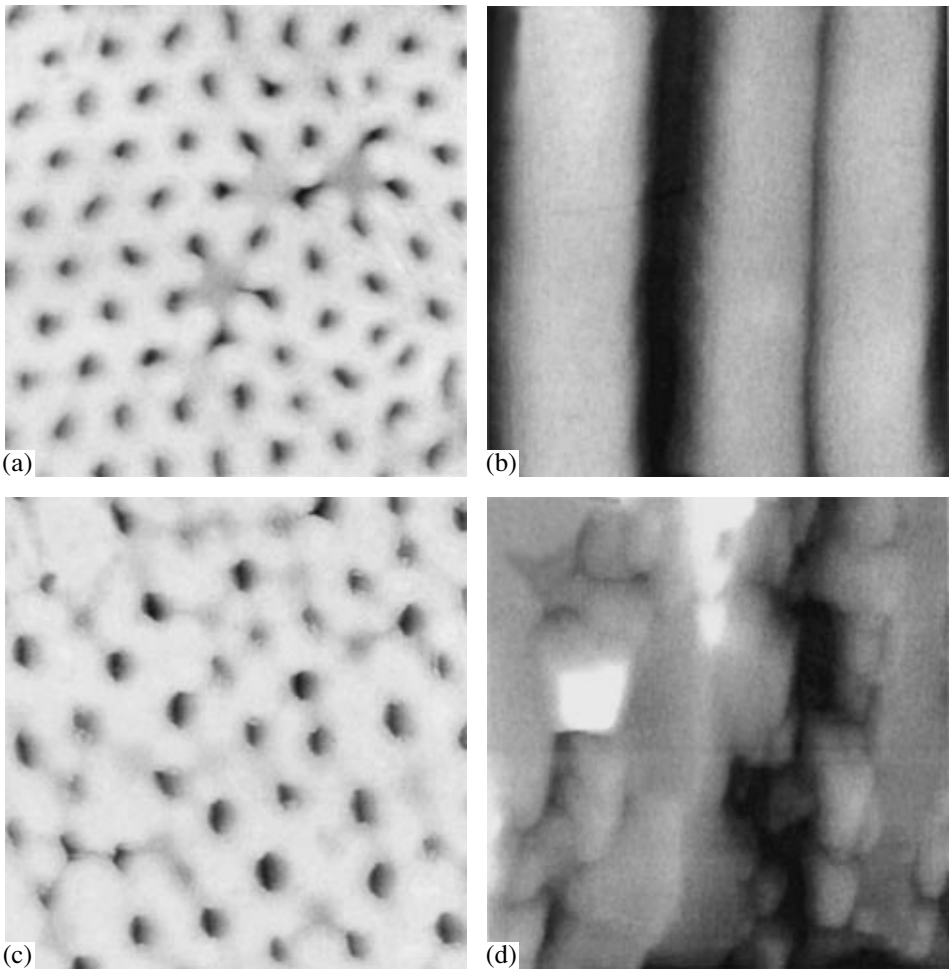

Fig. 1. AFM images of aluminum oxide membranes and ferroelectric/aluminum oxide composite nanostructures subjected to different treatments: (a, b) an unfilled membrane M_1 and a PZT/Al_2O_3 nanostructure M_1 (surface; the scanned area is 0.8×0.8 μm in size) and (c, d) an unfilled membrane M_2 and BST/Al_2O_3 nanostructure M_2 (cleavage; the scanned area is 1×1 μm in size).

annealed structures. The SH intensity from an unfilled membrane (irrespective of whether it is annealed or unannealed) is retained at a noise level as the angle of incidence varies. This means that the several-fold increase in the SH intensity, as well as the change in its angular dependence, is associated with the annealing of a pore-filling material. Since the annealing of a precursor results in crystallization of the perovskite phase, it is reasonable to assume that the nanocrystallites in the nanostructure are in the noncentrosymmetric (ferroelectric) phase in this case.

The obtained dependences of the SH intensity on the angle of incidence can be described by the effective-medium model with due regard for multipath interference. Since the 2D nanostructure in question is anisotropic, we used the Bruggeman model extended to anisotropic media [3] to describe the linear optical properties of the structure. In this model, the effective permittivity $\varepsilon_{ii}^{\text{eff}}$ of a medium consisting of elliptic nanoparticles (medium A) introduced into a matrix (medium B) can be determined from the equation

$$f_A\left[\frac{\varepsilon_A - \varepsilon_{ii}^{\text{eff}}}{\varepsilon_{ii}^{\text{eff}} + L_i(\varepsilon_i - \varepsilon_{ii}^{\text{eff}})}\right] + f_b\left[\frac{\varepsilon_B - \varepsilon_{ii}^{\text{eff}}}{\varepsilon_{ii}^{\text{eff}} + L_i(\varepsilon_B - \varepsilon_{ii}^{\text{eff}})}\right] = 0, \quad (1)$$

where f_A and f_B are the volume fractions; ε_A and ε_B are the permittivities of the A and B phases, respectively; and L_i is the anisotropic depolarizing factor (for cylinders, we used $L_x = L_y = 0.475$, $L_z = 0.05$ [3]). The nonlinear susceptibility was calculated as

$$\chi^{\text{eff}} = f_A\chi_A + f_B\chi_B. \quad (2)$$

The results of the numerical simulation are shown in Fig. 2b. The wavelength dependence of the SH intensity is determined by the wavelength dependences of the refractive indices of phases A and B and of the entire nanocomposite. The peaks in the angular dependences are caused by multipath interference.

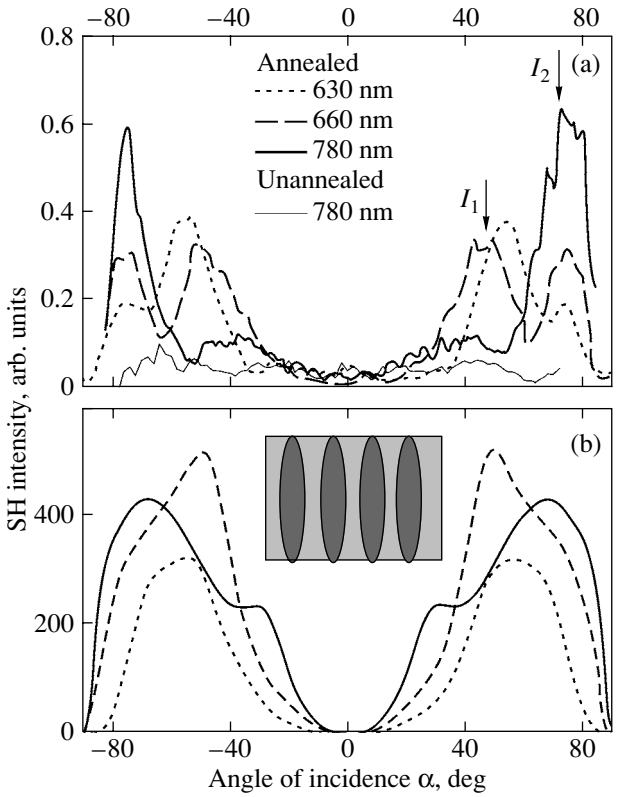

Fig. 2. (a) Experimental dependence of the SH intensity $I^{2\omega}(\alpha)$ on the angle of incidence of pump radiation for a PZT/Al_2O_3 nanostructure M_1 at different wavelengths and (b) the corresponding calculated dependence for the nanostructure model shown in the inset.

The numerical calculations qualitatively describe the experimental dependences of the SH intensity on the angle of incidence and their variation with the wavelength of light. However, in order to achieve quantitative agreement, further development of the model is required.

It should be noted that the experimental technique used in this study is applicable only to nanostructures that do not exhibit appreciable scattering.

3.2. Micro-Raman Scattering

BST/Al_2O_3 nanostructures M_2 were studied by micro-Raman spectroscopy (Fig. 3; curves *1*, *2* correspond to different points on the surface of the same structure). These structures are strongly scattering; however, this fact is not a handicap to micro-Raman scattering studies. In order to reveal the specific features in the Raman spectra of nanoparticles and matrices, the Raman spectra of nanostructures were compared with those of thin BST films prepared under identical conditions on various substrates.

The Raman spectra of thin BST films deposited on various substrates were found to be almost identical.

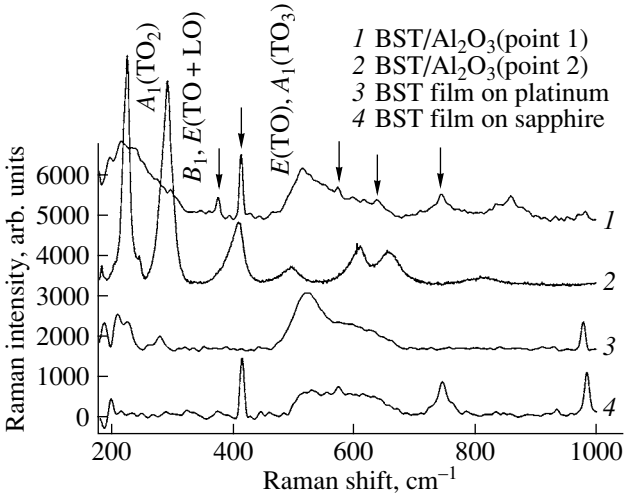

Fig. 3. Micro-Raman scattering spectra of (*1*, *2*) BST/Al_2O_3 composite nanostructures M_2, (*3*) a BST film on sapphire, and (*4*) a BST film on platinum. The Raman lines of Al_2O_3 are identified according to [5].

These spectra contain distinct broad peaks in the range 220–230 cm^{-1}, which can be identified as $A_1(TO_2)$ modes corresponding to transverse optical phonons, and broad asymmetric peaks in the range 500–600 cm^{-1} corresponding to the $E(TO)$ and $A_1(TO_3)$ phonon modes [4].

The Raman spectra of nanostructures, in contrast to the spectra of films, exhibit more pronounced features in these ranges. The spectra of nanostructures (points *1*, *2*) likewise exhibit distinctive features in the range 220–300 cm^{-1}. In the spectrum at point *1*, there is an asymmetric peak with maxima at 225 and 295 cm^{-1}, while the spectrum at point *2* has a pronounced peak at 295 cm^{-1}.

On the whole, the Raman spectrum at point *1* is closer to the spectrum of a film. The spectrum at point *2* has lines that are not characteristic of BST films of this composition [4]. A comparison of the Raman spectra at several points on the nanostructure surface shows that the surface is significantly inhomogeneous.

4. CONCLUSIONS

Thus, we have demonstrated the efficiency of the template technique for producing ferroelectric composite nanostructures. It has been shown that, in weakly scattering structures with small nanoparticles, the parameters of optical second harmonic generation are sensitive to the presence and amount of the ferroelectric phase, the filling factor, and the particle shape. Strongly scattering nanostructures cannot be studied using SH generation. However, the micro-Raman technique is applicable to scattering structures and makes it possible to study the homogeneity of structures with a spatial resolution of 1 μm.

ACKNOWLEDGMENTS

This study was supported by the Russian Foundation for Basic Research (projects no. 03-02-16945, 04-02-17248), the Ministry of Education and Science of the Russian Federation (project no. 84-43), and INTAS (grant no. 01-0075).

REFERENCES

1. F. D. Morrison, Y. Luo, I. Szafraniak, V. Vagarajan, R. B. Wehrspohn, M. Steinhart, J. H. Wendroff, N. D. Zakharov, E. D. Mishina, K. A. Vorotilov, A. S. Sigov, S. Nakabayashi, M. Alexe, R. Ramesh, and J. F. Scott, Rev. Adv. Mater. Sci. **4**, 1 (2003).
2. K. A. Vorotilov, M. I. Yanovskaya, E. P. Turevskaya, and A. S. Sigov, J. Sol–Gel Sci. Technol. **16**, 109 (1999).
3. J. Wang, J. Shao, and Z. Fan, Opt. Commun. **247**, 107 (2004).
4. S.-Y. Kuo, W.-Y. Liao, and W.-F. Hsieh, Phys. Rev. B: Condens. Matter **64**, 224103 (2001).
5. R. Krishnan, R. Kesavamoorthy, S. Dash, A. K. Tyagi, and B. Raj, Scr. Mater. **48**, 1099 (2003).

Translated by A. Kazantsev